CrossMark

Quantifying leaf-scale variations in water absorption in lettuce from hyperspectral imagery: a laboratory study with implications for measuring leaf water content in the context of precision agriculture

Richard J. Murphy[1] · Brett Whelan[2] · Anna Chlingaryan[1] · Salah Sukkarieh[1]

Abstract

Variations in water absorption across lettuce leaves (*Latuca sativa* L. var. *longifolia*) were quantified from hyperspectral imagery acquired in the laboratory using selected spectral indices, specifically, the Moisture Stress Index (MSI), the Normalised Difference Water Index (NDWI) and the intensity of specific water absorptions at 970 nm (IA_{970}), 1170 nm (IA_{1170}) and 1775 nm (IA_{1775}). Absorption was separately quantified for the midrib, the green parts of the leaves and for whole leaves. Indices were non-linearly related to water content expressed per weight of wet plant material (g g^{-1}) but linearly to water content per unit area of leaf (g cm^{-2}). Indices were weakly correlated with water content in the stem but strongly correlated with water in the green parts of leaves and in whole leaves. Water content in whole leaves was significantly underestimated ($P < 0.01$) when it was predicted from a model developed for the green parts of leaves, indicating that water content must be derived from the same leaf component used to derive the predictive model. Some indices (NDWI, MSI, IA_{1170}) highlighted intricate reticulated patterns of water absorption across the leaves but these were poorly defined by other indices (IA_{970}, IA_{1775}). Indices extracted from the leaf along transverse and longitudinal transects were qualitatively similar but quantitative analysis indicated that they were significantly different ($P < 0.05$). The principal contribution of this study is that it highlights the implications of quantifying leaf water content from hyperspectral imagery acquired at spatial resolutions great enough to resolve individual leaf components.

Keywords Hyperspectral imagery · Leaf water content · Absorption feature · Spectral indices · Precision agriculture

✉ Richard J. Murphy
richard.murphy@sydney.edu.au

1   The Australian Centre for Field Robotics, Department of Aerospace, Mechanical & Mechatronic Engineering, The University of Sydney, The Rose Street Building J04, Sydney, NSW 2006, Australia

2   Centre for Carbon, Water and Food, School of Life and Environmental Sciences, The University of Sydney, Sydney, NSW 2006, Australia

Introduction

In recent years, significant progress has been made on the use of hyperspectral imaging sensors in precision agriculture to provide growers with information relevant to the optimal management of their crops (reviewed by Sankaran et al. 2015). Hyperspectral imagery of crops acquired from an overhead perspective from aircraft or unmanned aerial vehicles (UAVs) have provided a wealth of information on crop biomass or yield (Wang et al. 2017; Liu et al. 2004; Yang et al. 2004; Yang and Everitt 2012), physiological functioning including indicators of stress (e.g. Ballester et al. 2017; Suárez et al. 2010; Zarco-Tejada et al. 2013a; Zarco-Tejada et al. 2012), nutrients in leaves (Cilia et al. 2014; Yu et al. 2014; Vigneau et al. 2011) and plant disease (Sankaran et al. 2010 and references therein; Mahlein et al. 2010). The usefulness of this information is constrained by numerous factors, including the spatial resolution of the sensor, the structure of the plant canopy and the proportion of soil and shade that is visible to the sensor, particularly where data are acquired at coarse spatial resolution (Zarco-Tejada et al. 2005; Takala and Mottus 2016; Zarco-Tejada et al. 2013b; Sims and Gamon 2003; Ollinger 2011). In the context of precision agriculture, hyperspectral data are increasingly being acquired from field-based or robotic platforms, resulting in significant increases in the spatial resolution of the data they collect (e.g. Underwood et al. 2017; Wendel and Underwood 2017). This increase in resolution opens up opportunities for detecting early signs of stress in plants at the scale of individual leaves before they become visible to the naked eye (Behmann et al. 2014).

One aspect of detecting stress in plants from hyperspectral data that has received considerable attention is the measurement of leaf water content. Several methods have been developed to measure water content from hyperspectral data acquired at wavelengths in the visible near-infrared (VNIR; 400–1000 nm) and shortwave-infrared (SWIR; 1000–2500 nm). Some methods, commonly based on spectral indices (e.g. Danson et al. 1992; Tian et al. 2001; Penuelas et al. 1993), have been designed to quantify the intensity of absorption (IA) of specific water absorption bands centred on 970 nm (IA_{970}), 1170 nm (IA_{1170}), 1450 nm (IA_{1450}), 1775 nm (IA_{1775}) and 1930 nm (IA_{1930}, Fig. 1). These specific absorptions, occurring across localised spectral regions, are superimposed onto a background of exponentially increasing water absorption towards longer wavelengths. The Water Index (WI), developed by Penuelas et al. (1997), quantifies the intensity of the water absorption at 970 nm and is equivalent to IA_{970}. Other methods such as the Moisture Stress Index (MSI; Hunt and Rock 1989) and the Normalised Difference Water Index (NDWI; Gao 1996) are based on ratios of reflectance across broad intervals of wavelengths aimed at quantifying the exponential increase in water absorption towards longer wavelengths, whilst minimising the effects of the soil background and the intervening atmosphere (Fig. 1). IA_{970} and NDWI have, in particular, been widely used in precision agriculture to quantify leaf water content in different crops, but largely at the canopy scale (e.g. Feng et al. 2017; Wang et al. 2015; Steidle Neto et al. 2017), and in other communities of vegetation (e.g. Serrano et al. 2000; Ding et al. 2017; Asner et al. 2005). Ceccato et al. (2001) found that reflectance in the SWIR was influenced not only by water absorption but also the internal leaf structure and dry matter content, including lingo-cellulose. These authors recommended that indices used to measure leaf water should include a band in the SWIR and a band in the VNIR, which is affected only by the internal leaf structure and dry matter, in order to normalise for these effects. The NDWI and MSI conform to this requirement but IA_{970} and other indices that quantify the specific water absorption bands do not (they use either VNIR or SWIR wavelengths, but not both). This has implications for measuring leaf water content in the context
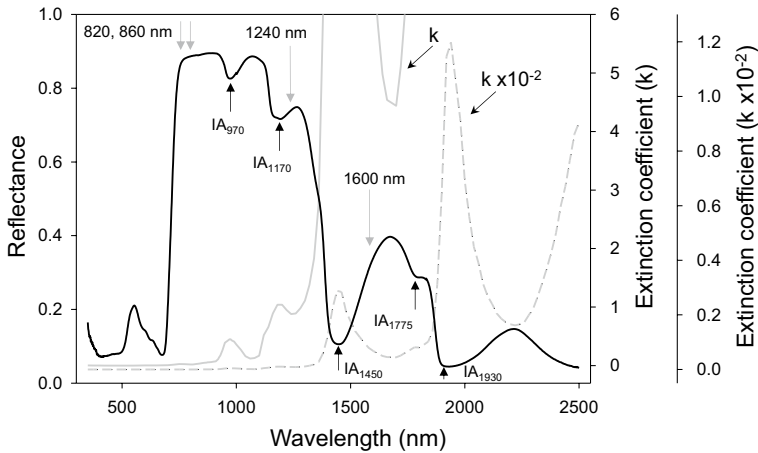
Fig. 1 Spectrum of a lettuce leaf (solid black line) showing the location of the water absorption features quantified in the study (IA_{970}, IA_{1170}, IA_{1775}; upward black arrows). Wavelengths used to calculate the NDWI and MSI are indicated (downward grey arrows). Coefficients of water absorption (k): original values (k; solid grey line); values scaled to show water absorptions towards shorter wavelengths ($k \times 10^{-2}$; dashed grey line)

of precision agriculture, because the vast majority of hyperspectral data are acquired using VNIR sensors, which are smaller, less expensive and measure wavelengths that are relevant for detecting plant stress and absorption by photosynthetic pigments. VNIR sensors are able to measure only one water index (IA_{970}); other indices can only be derived from SWIR data. It is useful therefore to understand the relationships between IA_{970} and other indices and, in particular, NDWI and MSI that normalise for effects of the internal leaf structure and lingo-cellulose by incorporating bands in the VNIR and SWIR.

Water absorption indices have been mainly developed and tested on non-imaging (i.e. discrete) spectral measurements of leaves (e.g. Gao 1996; Penuelas et al. 1997) or on spectra derived from radiative transfer models such as PROSPECT (Hunt et al. 2011; Wang et al. 2013). Indices are most often used with data acquired at canopy scales, i.e. where image pixels integrate spectral reflectance over surface areas that are substantially greater than that of individual leaves (e.g. Serrano et al. 2000; Yilmaz et al. 2008; Xiao et al. 2014). Accurate measurements of leaf water content at the canopy scale is therefore more challenging than for leaf-scale measurements because canopy scale measurements also include information from areas of bare soil, green and non-green components of plants, and shade. There are only a small number of studies (notably Kim et al. 2015; Pandey et al. 2017) that have used hyperspectral imagery to quantify absorption by water across the surface of individual leaves. Consequently, there are few data on how water is distributed at these scales and how this information may be used in detecting water stress.

The increased spatial resolution of hyperspectral data acquired from field based platforms brings with it new opportunities but also new challenges for data analysis. Acquisition of data at fine (< 2 mm) resolutions could provide important new information about how water is distributed within individual leaves, and how it may change in response to water stress. Such information has the potential to open up possibilities for the development of better precision indicators of water stress in plants, beyond those provided by gross measurements made at canopy scales. Moreover, because increasing

spatial resolution would allow individual leaf components to be detected, questions arise as to which plant tissues or areas on the leaf would yield the best estimates of water content. Given that different leaf tissues (e.g. midrib, green parts of leaves) are compositionally and/or structurally different, they would exhibit very different spectral characteristics, potentially leading to different estimates depending on which parts of the leaf were measured (Ollinger 2011). Furthermore, for some leaves on the plant, only their green parts may be visible to the imaging sensor, whilst for others, whole leaves may be visible (i.e. the midrib + the green parts of the leaves). Where hyperspectral data are spatially averaged to estimate water content at the leaf scale, this could mean that estimates are determined from hyperspectral observations comprising a mix of leaf components e.g. some proportion of the observations would be from the green part of leaves and others from whole leaves. In the worst case scenario, this could lead to a model describing the relationship between a hyperspectral index and leaf water content developed from one leaf component (e.g. the green parts of leaves) to be used, albeit inappropriately, for estimating water content across whole leaves. This raises important questions, not only about which leaf component should be sampled, but also about the consistency with which this must be done in order to minimise errors. Because all water indices are designed to detect water absorption, they should, theoretically, show similar spatial patterns of absorption across individual leaves. This, however, remains largely untested and would likely depend on how different indices are impacted by effects related to internal leaf structures and the lingo-cellulose content of the leaves (Ceccato et al. 2001; Dawson et al. 1998).

These questions are addressed here, using hyperspectral imagery of leaves of Romaine or Cos lettuce (*Latuca sativa* L. var. *longifolia*). Lettuce leaves are used in this study because they have large variations in structural water, distributed among different leaf components (e.g. the midrib and green parts of the leaves). Hyperspectral imagery acquired in the laboratory under artificial light is used in this study because it enables the performance of different indices to be evaluated without the effects of the intervening atmosphere; results therefore represent the 'best-case' scenario for estimating leaf water content from hyperspectral imagery.

This study has three objectives:

Objective 1   Determine the relationships between water indices and water content for different leaf components. Specifically, which water indices and which leaf component (i.e. the midrib, green parts of the leaves or whole leaves) provide the best measures of water content. Hypothesis 1: because all indices measure water content, they will have similarly strong relationships between measured water content among the different leaf components

Objective 2   Determine if a model derived from one leaf component can be used to estimate water content from data from a different leaf component. Hypothesis 2: leaf water content can be accurately estimated from indices from one leaf component (whole leaves) using a model developed for a different leaf component (the green parts of leaves)

Objective 3   Determine the relationships between indices. Hypotheses 3: because all indices have been designed to measure water content and therefore will contain similar information, indices will (a) show similar spatial patterns across leaves and (b) will have strong, positive and linear relationships with each other

The principal contributions of this study are to demonstrate that leaf-scale variations in water absorption can be quantified from VNIR and SWIR hyperspectral imagery using spectral indices and to highlight the implications for quantifying leaf water content acquired at spatial resolutions great enough to resolve individual leaf components.

Materials and methods

Leaf samples and acquisition of hyperspectral imagery

Hyperspectral images were acquired by separate hyperspectral imaging sensors (Specim Finland) to measure the VNIR (400–1000 nm) and the SWIR (1000–2500 nm) parts of the spectrum. The sensors were mounted on a scanning frame, pointing downwards onto a linear scanning table onto which the samples were placed. The sensors are line scanners, each containing a sensor array that measures one spatial dimension (the vertical or across track dimension) and all of the wavelengths recorded by the sensor. The second spatial dimension (the horizontal or along track dimension) is built up by moving the samples on the scanning table. Prior to imagery being acquired from the leaf samples, data (~1000 frames) were recorded from a reflectance standard (~99% Spectralon). The mean distance between the sensor objective and the samples was 550 mm, resulting in each square image pixel being ~0.72 mm. Two arrays of seven halogen lights each illuminated the samples from opposite directions on the scanning table. An appropriate integration time for each sensor was determined so that no pixels were saturated, i.e. they did not attain the maximal value represented by the bit-depth encoded by the respective sensor (12 and 14 bits, respectively for the VNIR and SWIR sensors). All sensor parameters used to acquire the hyperspectral images were kept constant across all scans.

Twenty, fresh 'Cos' lettuce plants were obtained directly from the farm with their root balls attached. The plants were kept under ambient light conditions with the root balls kept fully moist. Two plants were randomly selected for sampling for each of six hyperspectral scans (Table 1). Seven or eight leaves of similar size were detached from the plants and placed, using forceps, adjacently on a matt-black background for

Table 1 Details of the hyperspectral scans of the detached samples of leaves, their condition, time after detachment, number of leaves and whether water content was measured

Image scan	Leaf condition	Time after detachment (h)	Number leaves	Water content measured
1	Fresh	0	7	Yes
2	Fresh	0	7	Yes
3(1)[a]	Fresh	0	7	
3(2)[b]	Dehydrated	6 (D_6)	7	Yes
4	Fresh	0	7	Yes
5(1)[a]	Fresh	0	8	
5(2)[b]	Dehydrated	12 (D_{12})	8	Yes
6(1)[a]	Fresh	0	7	
6(2)[b]	Dehydrated	24 (D_{24})	7	Yes

[a]Scan before leaves dehydrated

[b]Scan after leaves dehydrated

scanning. Great care was taken not to exert any pressure on the leaves. Hyperspectral imagery was then immediately acquired from these samples (see below). Immediately after completion of some scans (scans 1, 2 and 4), leaves were immediately placed into individual plastic bags for independent determination of water content in the laboratory. After scans 3(1), 5(1) and 6(1) were completed, leaves were left in the same position on the scanning table to dehydrate for a period of 6, 12 and 24 h, respectively. Henceforth these data are termed D_6, D_{12} and D_{24}. A second scan was then acquired from the same leaves (scans 3(2), 5(2) and 6(2); Table 1). After completion of this second scan leaves were placed into individual plastic bags for determination of water content in the laboratory.

Hyperspectral images were corrected for dark current and calibrated to reflectance on a line-by-line basis. To do this, data from each across-track line were divided by data from the corresponding line from the calibration panel. This approach enabled small variations in incident illumination across the samples to be removed. Absolute reflectance was derived by multiplying the resulting quotient by the calibration panel reflectance factor for each spectral band.

Water indices

It was not desirable to consider exhaustively all spectral indices developed to measure water absorption. Five different water indices were selected for comparison (Table 2). NDWI and MSI were selected because they are commonly used and have been shown to be effective in quantifying vegetation water content at the canopy scale. Both these indices use wavelengths in the VNIR and the SWIR to quantify increasing absorption by water towards longer wavelengths whilst minimising effects related to internal leaf structure and lingo-cellulose (Ceccato et al. 2001; Dawson et al. 1998). The intensity of discrete water absorptions within atmospheric windows in the spectrum were also selected, specifically, IA_{970}, IA_{1170} and IA_{1775} (Fig. 1, Table 2). IA_{970} was selected because it is commonly used and lies within the visible near-infrared (VNIR; 400–1000 nm) range that is detected by most hyperspectral sensors used for precision agriculture. Although, IA_{1170} and IA_{1775} may be impacted by the internal structure of the leaf and dry matter (Ceccato et al. 2001), they are included here because they have been shown by some studies to be strongly correlated with water content (e.g. Tian et al. 2001; Sims and Gamon 2003). The intense water absorptions, IA_{1450} and IA_{1930}, were not considered in this study because they are not located in atmospheric windows and cannot normally be quantified from hyperspectral data acquired under natural illumination (but see Murphy 2015).

The intensity of IA_{970} nm was quantified by subtracting the reflectance at 970 nm from the reflectance at 900 nm and normalising this difference by the reflectance at 900 nm to make it comparable with measurements made from other features (Rollin and Milton 1998; Clark and Roush 1984). The intensities of IA_{1170} and IA_{1775} were quantified in the conventional way by first fitting a continuum across highpoints in the spectrum either side of each absorption. Wavelength intervals used in the process are given in Table 2. Normalised reflectance for each absorption was calculated by dividing the spectrum by the continuum. Intensity of absorption was then calculated as 1 minus the normalised reflectance at the absorption maximum, i.e. reflectance minimum (Clark and Roush 1984).

Table 2 Summary of water indices used in this study

Index	Abbreviation	Calculation[a]	Wavelength interval (nm)[b]	References
Normalised Difference Water Index	NDWI	$(R860 - R1240)/(R860 + R1240)$	—	Gao (1996)
Moisture Stress Index	MSI	$(R820 - R1600)/(R820 + R1600)$	—	Hunt and Rock (1989)
Absorption 1 (970 nm)	IA_{970}^{c}	$(R900 - R970)/R900$	—	Penuelas et al. (1997)
Absorption 2 (1170 nm)	IA_{1170}^{c}	$1 - Rnorm(min)^{d}$	1040–1324	Sims and Gamon (2003)
Absorption 3 (1775 nm)	IA_{1775}^{c}	$1 - Rnorm(min)^{d}$	1662–1849	Tian et al. (2001)

[a]R = wavelength of reflectance used in the calculation of index

[b]Wavelength interval over which normalised reflectance was calculated to derive the intensity of the feature

[c]IA = Intensity of absorption for the water absorption feature centred on that wavelength

[d]Rnorm(min) = Normalised reflectance at the absorption maximum (reflectance minimum) of the feature

Measurements of water in leaves

Gravimetric measurements of leaf water content were used for this experiment rather than measurements of stomatal conductance or leaf water potential because they provided a direct measurement of the water content of leaves. The 'Cos' lettuce used in this study comprised a large fleshy midrib from which several fine lateral veins extended outwards towards the leaf boundary. Finely reticulated veins were present between the lateral veins. In the laboratory, each leaf was removed in turn from its plastic bag and the large midrib removed from the leaf with a scalpel. The midrib and green, photosynthetic parts of the leaf were weighed separately and placed into individual paper bags for drying. Excised midribs and leaves were dried for a period of 18 h in an oven at 60° C and then reweighed. The area of each leaf was determined directly from the hyperspectral imagery.

Amounts of water in the midribs and leaves was determined and expressed in grams per unit weight of wet plant material $(g\ g^{-1})$ and in grams per unit leaf area $(g\ cm^{-2})$:

$$\text{Water content per unit weight} \left(g\ g^{-1}\right) = (\text{wet weight} - \text{dry weight}) / \text{wet weight} \tag{1}$$

$$\text{Water content per unit area} \left(g\ cm^{-2}\right) = (\text{wet weight} - \text{dry weight}) / \text{leaf area} \tag{2}$$

Analyses of data

To determine which hyperspectral water indices and which leaf component provide the best measures of water content (Objective 1), regression analysis was used to describe relationships between water content and each water index. Where water content needed to be estimated from the indices, the regression equation was inverted. Non-linear and ordinary least squares regression were used, respectively, to describe relationships for water content expressed per unit weight of plant material $(g\ g^{-1})$ and per unit area of leaf $(g\ cm^{-2})$. Note that in all graphs where index values for different leaf components are plotted as a function of measured water content, data are matched for that component e.g. index values for the midrib are plotted against water content from the midrib.

To determine if a model derived from one leaf component can be used to estimate water content from data from a different leaf component (Objective 2), water content $(g\ cm^{-2})$ was estimated from index data from whole leaves using a model developed for (i) green leaves (WL-P-GL; i.e. the model was for a different leaf component) and, separately, from a model developed for whole leaves (WL-P-WL; i.e. the model was from the same leaf component). Separate analyses of variance (ANOVA) were used to test for significant differences between estimates provided by WL-P-GL and WL-P-WL for each index. ANOVA was used to test for significant differences in estimates provided by WL-P-GL and WL-P-WL among all indices; Student–Newman–Keuls (SNK) tests were used to test for pairwise differences between indices.

Orthogonal regression was used to determine the nature and strength of relationships between pairs of water indices (Objective 3). Orthogonal regression was used in preference to ordinary least squares regression because all indices were measured with error. Similarity in spatial patterns of index values across leaves were evaluated for the seven fresh leaves in image scan 1. For each leaf, index values along two transverse and two longitudinal transects were extracted from the image (resulting in 14 transverse and 14 longitudinal transects in total). The transverse transects extended from one side of each leaf

to the other, across the midrib; the longitudinal transects were positioned approximately halfway between the midrib and the edge of the leaves, running from their base (the point of attachment to the plant) to the apex. After rescaling all index values to between 0 and 1, the similarity between all possible pairs of indices were compared within each transect, by measuring the angle (in radians) between their vectors, using the spectral angle mapper (Kruse et al. 1993). Smaller angles (0 indicating a perfect match) indicate that the patterns of changing index values along each transect were similar or vice versa. Thus, for each pair of indices there were 14 replicate angular measurements for each transect. Average values were then assembled into a confusion matrix showing the similarity between all pairs of indices. ANOVA was used to test for significant differences among indices and SNK tests were used for pairwise comparisons.

Results

Spectral characteristics of fresh leaf components

Averages of all pixels within each leaf component were used to compare reflectance spectra across all stages of dehydration (Fig. 2). In fresh leaves and at all stages of dehydration (D_6, D_{12} and D_{24}), reflectance spectra of the midrib were markedly different from the green parts of the leaves and from whole leaves. Reflectance in the visible range was greater, and the rise in reflectance between the red and NIR was much smaller compared with the green and whole leaf components. Reflectance at wavelengths > 1200 nm was also smaller. Spectra of the green and whole leaf components were very similar. With increasing time of dehydration, reflectance of green and whole leaf components increased across wavelengths > ~ 1200 nm, but decreased in the midrib (see values at 1700 nm, given above each spectrum in Fig. 2). Variability in reflectance among individual leaves for the green and
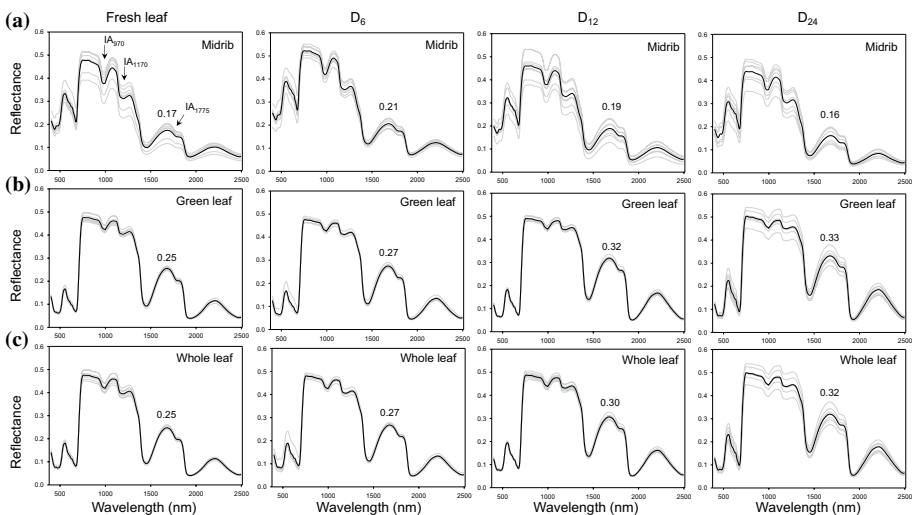
Fig. 2 Individual (grey lines) and average (black line) reflectance spectra (400–2500 nm) for individual leaf components for fresh leaves, and leaves dehydrated for 6 (D_6), 12 (D_{12}) and 24 (D_{24}) hours: **a** midrib; **b** green parts of the leaves and **c** whole leaves (midrib + green parts of the leaves)

whole leaf components increased at time D_{24}, compared with fresh leaves and leaves dehydrated for shorter periods of time (D_6 and D_{12}; see grey lines in Fig. 2).

Relationships between water indices and water content for different leaf components (Objective 1)

For the midrib, weak, non-linear relationships were found between all index values and water content per unit weight (g g^{-1}; Fig. 3a, Table 3). Relatively large changes in index value occurred across a relatively small range of values of measured water content. Strong non-linear relationships were found between index value and water content (g g^{-1}) in the green and whole leaf components (Fig. 3b, Table 3). Similar to the midrib component, large changes in index value occurred across a small range of values representing water content, especially where these values were large. At smaller values of water content, the opposite was found with large changes occurring across a relatively small range of index values. Relationships between index values and water content (g g^{-1}) for all leaf components were best described by an exponential growth model with three parameters:

$$y = y0 + a * \exp(b * x)$$
(3)

where y0 is the point where the asymptote crosses the y-axis, a is the intercept minus y0 and b is the rate of change.

Weak to moderately strong linear relationships were found between water content per unit area of leaf (g cm^{-2}) and NDWI, MSI, IA_{970} and IA_{1170} measured in the midrib (Fig. 4, Table 4). There was no relationship between water content (g cm^{-2}) and IA_{1775}. For the green and whole leaf components, strong linear relationships were found between water content (g cm^{-2}) and all index values. With the exception of NDWI, the slope and intercept of the regression for the green leaf component were significantly different from those of the whole leaf component (analysis of covariance; ANCOVA; $P < 0.05$; bold text in Table 4). The difference in the slope describing the relationship between water content and index was greater for those indices using longer wavelengths. For example, the difference in
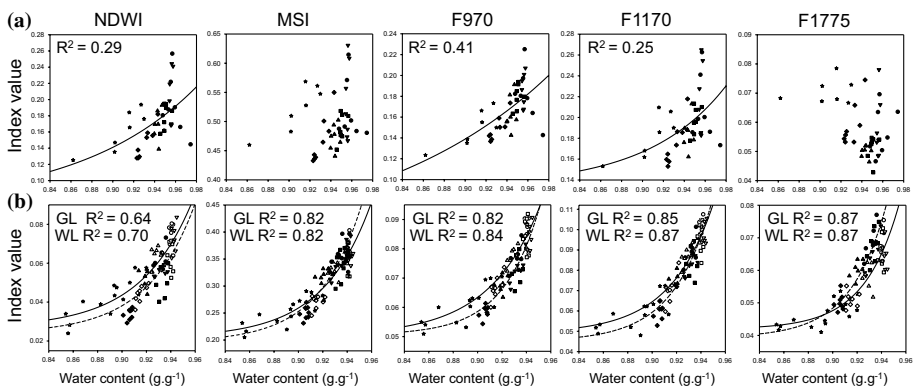
Fig. 3 Regression of index value on water content per unit weight (g g^{-1}) of leaf: **a** midrib, **b** green parts of the leaves (solid symbols) and whole leaves (open symbols). Different symbols represent data from different image scans (see Table 1): Scan 1 (circle); Scan 2 (square); Scan 3(2)[b] (triangle); Scan 4 (inverted triangle); Scan 5(2)[b] (diamond); Scan 6(2)[b] (star). Lines of best fit for the green parts of the leaves (dashed line) and for the whole leaves (solid line) are shown

Table 3 Relationships between water content (per gram of plant material; g g^{-1}) and intensity of water absorption measured by different indices: (a) midrib; (b) green parts of the leaves and (c) in whole leaves

Index	R^2	SE	P	y0	a	b
(a)						
NDWI	0.29	0.027	< 0.01	0.068	2.45E−5	8.87
MSI	—	—	—	—	—	—
IA$_{970}$	0.41	0.017	< 0.0001	0.036	0.0005	5.84
IA$_{1170}$	0.25	0.024	< 0.01	0.134	1.85E7	13.43
IA$_{1775}$	—	—	—	—	—	—
(b)						
NDWI	0.64	0.007	< 0.0001	0.023	1.34E−12	25.65
MSI	0.82	0.020	< 0.0001	0.196	2.70E−13	28.96
IA$_{970}$	0.82	0.004	< 0.0001	0.050	7.32E−16	33.36
IA$_{1170}$	0.85	0.006	< 0.0001	0.042	6.11E−14	29.24
IA$_{1775}$	0.87	0.004	< 0.0001	0.038	1.27E−15	32.94
(c)						
NDWI	0.70	0.008	< 0.0001	0.026	1.12E−11	23.46
MSI	0.82	0.020	< 0.0001	0.204	7.36E−12	25.26
IA$_{970}$	0.84	0.004	< 0.0001	0.050	6.24E−12	23.85
IA$_{1170}$	0.87	0.006	< 0.0001	0.046	1.85E−12	25.56
IA$_{1775}$	0.87	0.004	< 0.0001	0.040	1.05E−14	30.30
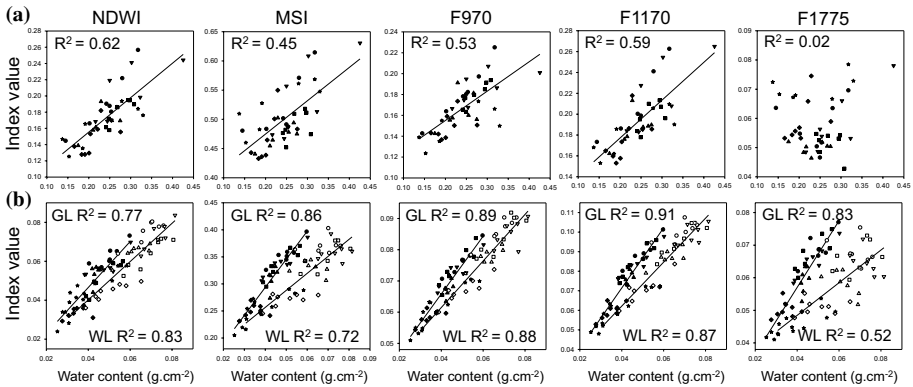
Fig. 4 Regression of index value on water content per unit area (g cm^{-2}) of leaf: **a** midrib, **b** green parts of the leaves (GL; solid symbols) and whole leaves (WL; open symbols). Different symbols represent data from different image scans (see Table 1): Scan 1 (circle); Scan 2 (square); Scan 3(2)[b] (triangle); Scan 4 (inverted triangle); Scan 5(2)[b] (diamond); Scan 6(2)[b] (star). Lines of best fit for the green parts of the leaves (dashed line) and for the whole leaves (solid line) are shown

slope between green and whole leaf components for MSI (that uses reflectance at 1660 nm) was greater than for NDWI (that uses reflectance at 1240 nm). Furthermore, differences in slope progressively increased with increasing wavelength used in those indices quantifying the intensity of discrete water absorptions (i.e. IA$_{970}$, IA$_{1170}$ and IA$_{1775}$). The strong linear relationships between water content expressed per unit area (g cm^{-2}) and all indices made these models (and the estimates derived from them) easier to interpret than the non-linear

Table 4 Relationships between percent water content (per unit area of leaf; g^{-1} cm^{-2}) and intensity of water absorption measured by different indices: (a) midrib; (b) green parts of the leaves and (c) whole leaves

| Index	R^2	SE	P	slope	intercept
(a)					
NDWI	0.62	0.020	< 0.0001	0.420	0.070
MSI	0.45	0.036	< 0.0001	0.570	0.360
IA_{970}	0.53	0.010	< 0.0001	0.280	0.100
IA_{1170}	0.59	0.020	< 0.0001	0.360	0.100
IA_{1775}	0.02	—	—	—	—
(b)					
NDWI	0.77	0.005	< 0.0001	1.180	0.000
MSI	0.86	0.018	< 0.0001	**5.187**	**0.086**
IA_{970}	0.89	0.003	< 0.0001	**0.927**	**0.029**
IA_{1170}	0.91	0.004	< 0.0001	**1.538**	**0.010**
IA_{1775}	0.83	0.004	< 0.0001	**1.023**	**0.016**
(c)					
NDWI	0.83	0.005	< 0.0001	0.980	0.000
MSI	0.72	0.025	< 0.0001	**3.145**	**0.130**
IA_{970}	0.88	0.004	< 0.0001	**0.747**	**0.032**
IA_{1170}	0.87	0.006	< 0.0001	**1.124**	**0.017**
IA_{1775}	0.52	0.006	< 0.0001	**0.501**	**0.028**

models. For this reason, all further analyses were done using models derived from water content expressed per unit area (g cm^{-2}).

Using a model derived from one leaf component to estimate water content from data from a different leaf component (Objective 2)

For all indices, water content estimated from whole leaves using a model derived for the green parts of the leaves (WL-P-GL) were significantly smaller than estimates obtained by using a model derived from the same leaf component (WL-P-WL; in all cases $P < 0.01$; Fig. 5a; Table 5). Where the model used for the prediction was derived from the same leaf component as the data used in the prediction (WL-P-WL), estimates of leaf water content across all indices were consistent (0.0609). Difference in estimates derived by WL-P-GL and WL-P-WL were significant among indices, with some indices showing much greater differences than others, e.g. differences from IA_{1775} were much greater than those from IA_{970} (results from SNK tests are shown at the top of Fig. 5a). Differences in estimates provided by WL-P-GL and WL-P-WL, expressed as a percentage of the measured range of water content, ranged from ~ 19% (IA_{970}) to ~ 37% (IA_{1775}; Table 5). With increasing amount of measured water, the differences between estimates derived by WL-P-GL and WL-P-WL increased (Fig. 5b).

Relationships between water indices (Objective 3)

Qualitatively, the spatial distributions of water absorption as measured by different indices were broadly similar, but showed important differences (Fig. 6). All indices highlighted large variations in absorption by water across the leaves, with leaf veins having greater
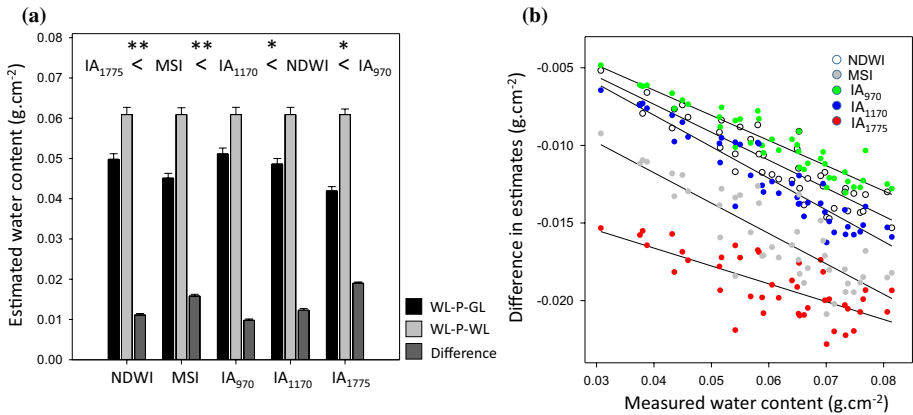
Fig. 5 Differences in amounts of water (g cm^{-2}) estimated from whole leaves by WL-P-GL and WL-P-WL: **a** Differences between WL-P-GL and WL-P-WL for each index. Results from SNK tests showing significant differences among indices are indicated (top; $P=0.95$(*), $P=0.99$(**)); **b** Difference in estimates for each index as a function of measured amounts of water in whole leaves (Color figure online)

Table 5 Average amounts of water (g cm^{-2}) and standard error (SE) derived from WL-P-GL and WL-P-WL (see text for details and Fig. 5a)

Index	Mean (SE) WL-P-GL	Mean (SE) WL-P-WL	Mean difference	% of measured range
NDWI	0.0498 (0.0014)	0.0609 (0.0018)	0.011	21.93
MSI	0.0451 (0.0012)	0.0609 (0.0017)	0.016	31.27
IA$_{970}$	0.0511 (0.0015)	0.0609 (0.0018)	0.010	19.40
IA$_{1170}$	0.0486 (0.0014)	0.0609 (0.0018)	0.012	24.28
IA$_{1775}$	0.0419 (0.0011)	0.0609 (0.0014)	0.019	37.53

absorption than areas of the leaf that were visually green. Veins in the leaf highlighting variations in water absorption comprised the central midrib, lateral veins extending from the midrib to the borders of the leaf and fine, complex, reticulated veins connecting the lateral veins. Reticulated veins were highlighted by NDWI, MSI and IA$_{1170}$ (Fig. 6b, c, e) but were poorly resolved in colour imagery and by IA$_{970}$ and IA$_{1775}$ (Fig. 6a, d, f). Many veins that were not readily visible in the colour imagery, were resolved by the water indices (cf. Fig. 6a–f). With the exception of IA$_{1775}$, the largest index values were found in the midrib of each leaf. IA$_{1775}$ showed decreased index values in the midrib, suggesting that water absorption was smaller in this area than in the other parts of the leaves. Specular and topographic self-shading effects caused by fine-scale wrinkles on the leaf surface were effectively removed by all indices. Inspection of these images showed that different indices conveyed different information about water absorption in leaves. NDWI, MSI and IA$_{1170}$ showed similar spatial patterns of water absorption, however, these were different to IA$_{970}$ and IA$_{1775}$.
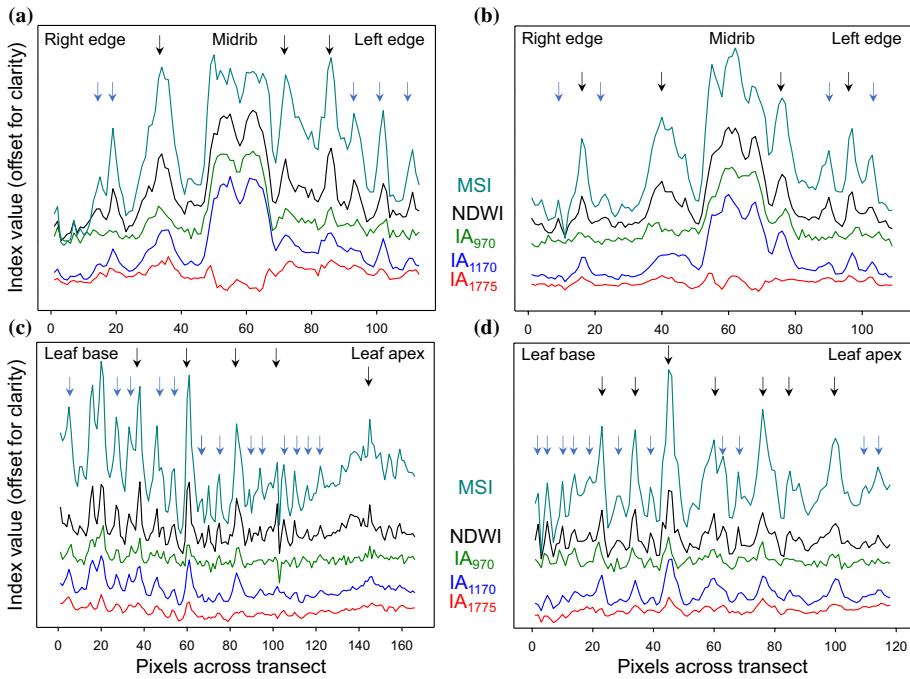
Plots of index values along transverse and longitudinal leaf transects (location of transects are shown for leaf #3 in Fig. 6a) showed that NDWI, MSI, IA$_{970}$ and IA$_{1170}$ had broadly similar patterns, with peaks and troughs in index values being located at the same
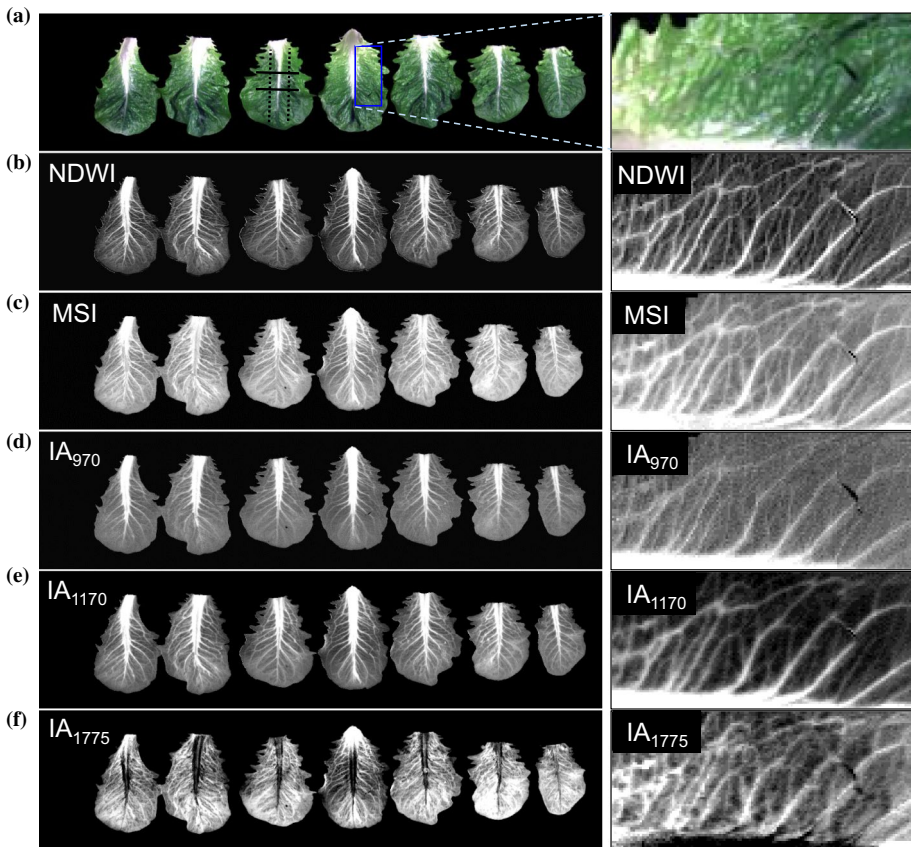
Fig. 6 Example colour image (Image scan 1) and derived indices from detached lettuce leaves: **a** Colour image; **b** NDWI; **c** MSI; **d** IA_{970}; **e** IA_{1170}; **f** IA_{1775}. Pixel values (brightness) are proportionate to value of each index. A zoomed area of leaf #4 is shown on the right (area shown as a rectangle in (**a**)). The location of the transverse (solid black line) and longitudinal (dashed line) transects used matching spatial patterns are shown for leaf #3 in (**a**) (Color figure online)

or similar distances along the transects (Fig. 7). The amplitude of peaks varied among these indices, with MSI and IA_{970} having the greatest and smallest amplitude, respectively. The relative heights of the peaks were also different among the indices. Peaks of similar height in one index (e.g. MSI) had different relative heights in other indices (e.g. cf. MSI and IA_{970}; Fig. 7a). IA_{1775} showed a pattern that was different to all other indices, particularly in the transverse transects which crossed the midrib (Fig. 7a, b). Values of IA_{1775} over the midrib showed the opposite pattern to other indices, decreasing with respect to adjacent areas of the leaves. For other veins in the leaves (i.e. the smaller lateral and reticulated veins), peaks and troughs of IA_{1775} values were broadly coincident with other indices, albeit at a much smaller amplitude.

Similarity between pairs of indices along the leaf transects, as measured by the spectral angle, were different for the transverse and longitudinal profiles (Table 6). For example, on average, the profiles of NDWI were most similar to profiles of IA_{1170}, MSI and IA_{970} in the transverse transect (i.e. their angles were small), but in the longitudinal transects, profiles

Fig. 7 Index values along longitudinal and transverse transects of freshly detached, green leaves. **a** Transverse transect (leaf # 4; Image 1; see Table 1); **b** Transverse transect (leaf # 4; Image 3(1)); **c** Longitudinal transect (leaf 4; Image 1); **d** Longitudinal transect (leaf 4; Image 3(1)). The location of lateral and reticulated veins in the leaves are indicated by black and blue downward arrows, respectively (Color figure online)

Table 6 Similarity (spectral angle) between profiles of indices extracted along longitudinal and transverse transects from leaves (left panel) and the significance (pairwise SNK tests) of mean differences in similarity between indices (right panel); $P < 0.05$ (*), $P < 0.01$ (**)

Transverse transects

	NDWI	MSI	IA$_{970}$	IA$_{1170}$
MSI	0.25			
IA$_{970}$	0.26	0.43		
IA$_{1170}$	0.19	0.32	0.23	
IA$_{1775}$	0.79	0.59	0.92	0.86

Most similar → Least similar

NDWI	vs.	IA$_{1170}$	* <	MSI	=	IA$_{970}$	** < IA$_{1775}$
MSI	vs.	IA$_{1170}$	** <	IA$_{970}$	** <	IA$_{1775}$	
IA$_{970}$	vs.	IA$_{1170}$	** <	IA$_{1775}$			
IA$_{1170}$	vs.	IA$_{1775}$	No test.				

Longitudinal transects

	NDWI	MSI	IA$_{970}$	IA$_{1170}$
MSI	0.18			
IA$_{970}$	0.31	0.29		
IA$_{1170}$	0.23	0.16	0.30	
IA$_{1775}$	0.38	0.24	0.40	0.35

Most similar → Least similar

NDWI	vs.	MSI	** <	IA$_{1170}$	** <	IA$_{970}$	** < IA$_{1775}$
MSI	vs.	IA$_{1170}$	** <	IA$_{1775}$	** <	IA$_{970}$	
IA$_{970}$	vs.	IA$_{1170}$	** <	IA$_{1775}$			
IA$_{1170}$	vs.	IA$_{1775}$	No test.				

of NDWI were most similar to MSI and IA_{1170}. In the transverse transect, profiles of IA_{1775} were not similar to profiles of any other index i.e. spectral angles were very large (≥ 0.59) but in the longitudinal transect, IA_{1775} did show a much greater similarity with MSI, compared with the other indices. The large angles between IA_{1775} and all other indices in the transverse transects can be attributed to the smaller values of IA_{1775} over the midrib (see Figs. 6, 7a, b). Although there was relative similarity between the profiles of some pairs indices in the longitudinal transects, as indicated by their small spectral angles, SNK tests showed that there were significant differences in similarity between them (Table 6; right panel). In the transverse transects, all profiles of indices were significantly different with the exception of MSI and IA_{970} which were statistically equal to each other when compared with NDWI.

Relationships between indices from different leaf components were visualised by creating a confusion matrix showing index values from the midrib (M) and green parts of leaves (GL; Fig. 8). Correlations between some pairs of indices across whole leaves (WL) were
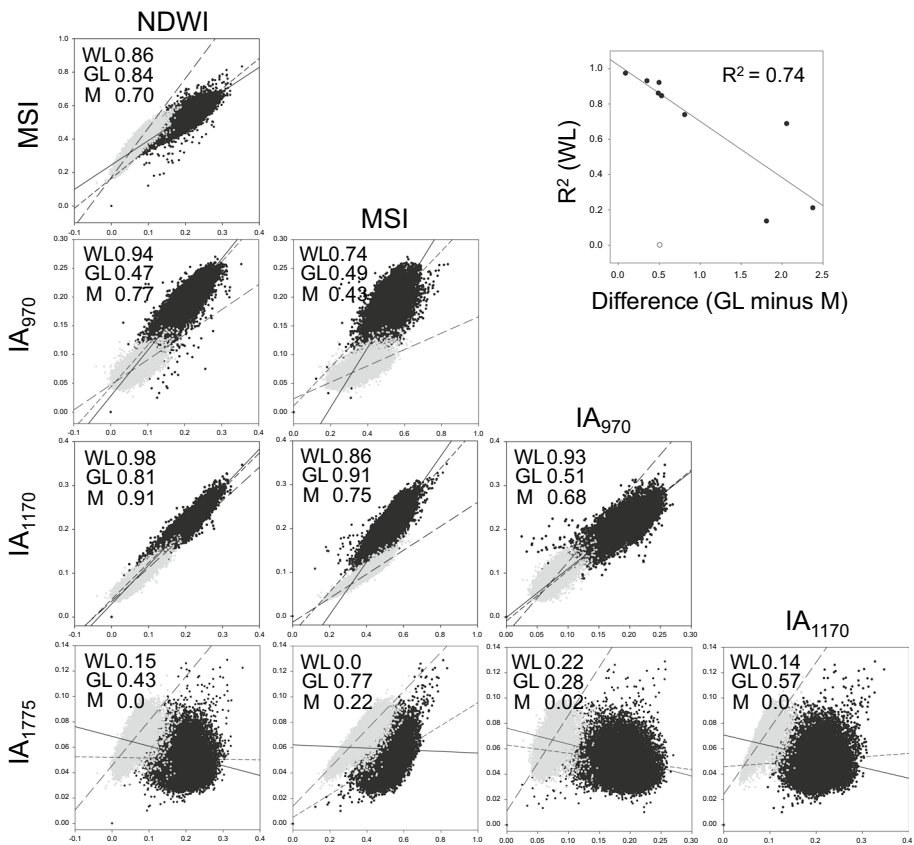
Fig. 8 Confusion matrix showing relationship between water indices determined from the midrib (black symbols) and the green parts of the leaves (grey symbols). The lines of best fit and coefficient of determination (R^2) derived from orthogonal regression are shown (WL; solid line), the green parts of leaves (GL; long dash) and the midrib (M; short dash). R^2 values for WL decreases with increasing difference in slope between GL and M (inset). Outlier shown as open circle is not included in calculation of R^2 (shown at upper right of inset)

strong, specifically: NDWI and IA_{970} ($R^2 = 0.94$), NDWI and IA_{1170} ($R^2 = 0.98$), and IA_{970} and IA_{1170} ($R^2 = 0.93$). The weakest correlations were found between IA_{1775} and all other indices ($R^2 \leq 0.22$). Relationships between indices were different for different leaf components, with the indices from the midrib having, in most cases, a very different relationship to indices from the green parts of leaves. For example, the relationship between MSI and IA_{970} had a different slope and intercept for the midrib (short dashed line) and the green parts of leaves (long dashed line) and both were different from the relationship for the whole leaves (solid line; Fig. 8). The relationship between NDWI and IA_{1170} was the exception, with relationships for the midrib, green parts of leaves and whole leaves (WL) being similar. The strength of relationships (R^2) between indices across whole leaves were dependent upon the difference in slopes that describe relationships between indices from the green parts of leaves and the midrib. With increasing difference in slope between the green parts of leaves and the midrib there is a progressive decrease in R^2 for whole leaves (inset; Fig. 8).

Relationships between IA_{1775} and other indices were very different to that for all other pairs of indices (Fig. 8). IA_{1775} was the only index that was negatively correlated with other indices (i.e. relationships had a negative slope). This was caused by pixels in the midribs having, on average, a relatively smaller IA_{1775} index values than in the rest of the leaves. For all other indices, pixels in the midribs had the greatest index value of all leaf components.

Discussion

Water indices derived from hyperspectral images are strongly and linearly related to water content expressed per unit area of leaf (g cm^{-2}) but not per gram of plant material (g g^{-1}). Non-linear relationships between water indices and water content expressed in grams per unit weight of plant material are likely caused in part by light penetrating to variable depths within the leaves, a factor that depends on the type and thickness of plant tissues through which it passes. Furthermore, measurements of plant material, used in the calculation of water content per unit weight of plant material (g g^{-1}), are obtained using the whole thickness of the midrib or leaf, across a distance where plant tissues may be of variable density. Comparison of remote sensing measurements made at the surface (or integrated across some unknown depth from it), with weight-based measurements (integrated over the total thickness of leaves) is likely to cause non-linear effects, as was observed for intertidal sediments by Murphy et al. (2005).

Indices describing the intensity of specific water absorptions in the spectrum (IA_{970}, IA_{1170}, IA_{1775}) use only wavelengths in the relatively narrow spectral regions in which they are located. The exponential increase in water absorption towards longer wavelengths has implications for the use of specific absorptions located at longer wavelengths (e.g. IA_{1775}) as an index of water content. The large increases in absorption background towards longer wavelengths flattens the absorption near 1775 nm by depressing reflectance across the whole feature, including its shoulders, thus reducing the intensity of the feature as water content increases. Additionally, absorption by lingo-cellulose may also have had an impact on the intensity of IA_{1775} (Dawson et al. 1998 and references therein). These finding are consistent with those of other researchers who found that the wavelengths that were most strongly correlated with water content were those where water most weakly absorbed and vice versa (Danson et al. 1992; Sims and Gamon 2003).

Intricate spatial patterns in water absorption across the leaves were revealed by the indices, which effectively normalised brightness variations and specular effects caused by the wrinkled leaf surfaces. NDWI and MSI resolved fine-scale reticulated patterns of water absorption, however, these were not well resolved by IA_{970} or IA_{1775}. For IA_{970} the likely cause of this is an increase in noise due to a falloff in sensitivity towards the longwave limit (1000 nm) detected by the VNIR hyperspectral sensor. For IA_{1775}, the lack of fine-scale structure is most likely due to variability in absorption by dry plant material, including lingo-cellulose in the leaf tissues. Because IA_{1775} uses only wavelengths around the location of this absorption feature (1662–1849 nm), normalisation for absorption by dry plant material (using a VNIR band) is not done. These factors may partly explain the differences in spatial patterns along the leaf transects. The findings of this study have implications for the use of hyperspectral data for estimating leaf water content in the context of precision agriculture, particularly where crops have leaves where a significant proportion of the leaf is occupied by a thick, fleshy midrib (as in the case of lettuce). The present study used hyperspectral imagery acquired in the laboratory under artificial light because it removed any variability caused by atmospheric effects. Results presented here therefore represent the best case scenario for measuring leaf water content using hyperspectral imagery. All water absorptions, by definition, are impacted by atmospheric water absorption, which reduces the amount light detectable by sensors. When coupled with decreasing solar output towards longer wavelengths and loss of sensitivity of sensors towards the limits of their sensed spectral range, atmospheric water absorption can significantly reduce the signal-to-noise ratio of the data and increase errors in estimates of water absorption.

The increasing use of hyperspectral data to inform growers of changes in the physiological status of crops will open up new opportunities for their use in precision agriculture. This paper, one of the first to quantify absorption by individual leaves across their surfaces using a combination of VNIR and SWIR wavelengths, shows that consistent measurements of leaf water content are dependent on the choice of index and the use of appropriate protocols for sampling image data at leaf scales.

Conclusions

(1) Non-linear relationships were found between leaf water content expressed per unit weight of plant material ($g\ g^{-1}$) and all indices. Relationships were linear where water content was expressed per unit area ($g\ cm^{-2}$) of leaf. Weaker relationships were found between indices and water content in the midrib than for the green parts of leaves or whole leaves. The linearity and strength of the relationship between the indices and water content per unit area ($g\ cm^{-2}$) makes it a more suitable measure than water content per unit weight ($g\ g^{-1}$).

(2) IA_{970} and IA_{1170} has the strongest correlations with water content ($g\ cm^{-2}$) of all the indices, including the more sophisticated indices that used both VNIR and SWIR bands (i.e. NDWI, MSI). IA_{1775} was strongly related to water content ($g\ cm^{-2}$) in the green parts of leaves but not in whole leaves. Hypothesis 1, that all indices will have similarly strong relationships with water content is therefore rejected.

(3) Leaf water content was significantly underestimated ($P < 0.01$) if it was predicted from average index values from whole leaves using a model developed for the green parts of leaves. Hypothesis 2 that leaf water content can be estimated from indices from one leaf component (whole leaves) using a model developed for a different leaf component

(green parts of leaves) is therefore rejected. Thus, if indices are to be comparable across time or space they should best be extracted from the same leaf component.

(4) Intricate, reticulated patterns of water absorption were highlighted by NDWI, MSI and IA_{1170}. Reticulated patterns were less evident in IA_{970} and IA_{1775} probably due to spectral noise and absorption by dry matter, respectively. Resolution of variations in absorption across leaves opens up the possibility for developing new methods to detect stress based on changes in patterns of water absorption across leaves.

(5) Indices extracted along transverse and longitudinal transects from the leaves showed significantly different spatial patterns along the transects. Consistent with qualitative observations of spatial patterns of index values (Conclusion 4), NDWI, MSI and IA_{1170} had, on average, the greatest similarity of patterns along the transects. Patterns of IA_{1775} along the transects were different to other indices. Hypothesis 3(a) that indices will show similar spatial patterns across leaves is therefore rejected.

(6) Some pairs of indices were strongly correlated but others were not. The strongest correlations were found between NDWI and IA_{970} and IA_{1170}. IA_{1775} was weakly correlated with all other indices indicating that, at the leaf scale, IA_{1775} did not contain the same information as other indices and should be interpreted with great caution. Weak correlations between indicates were attributed to differences in the relationships between the midrib and the green parts of leaves. Thus, Hypothesis 3(b) that all indices will have strong, positive and linear relationships with each other is rejected.

References

Asner, G. P., Carlson, K. M., & Martin, R. E. (2005). Substrate age and precipitation effects on Hawaiian forest canopies from spaceborne imaging spectroscopy. *Remote Sensing of Environment, 98*(4), 457–467. https://doi.org/10.1016/j.rse.2005.08.010.

Ballester, C., Zarco-Tejada, P. J., Nicolás, E., Alarcón, J. J., Fereres, E., Intrigliolo, D. S., et al. (2017). Evaluating the performance of xanthophyll, chlorophyll and structure-sensitive spectral indices to detect water stress in five fruit tree species. *Precision Agriculture*. https://doi.org/10.1007/s11119-017-9512-y.

Behmann, J., Steinrücken, J., & Plümer, L. (2014). Detection of early plant stress responses in hyperspectral images. *ISPRS Journal of Photogrammetry and Remote Sensing, 93,* 98–111. https://doi.org/10.1016/j.isprsjprs.2014.03.016.

Ceccato, P., Flasse, S., Tarantola, S., Jacquemoud, S., & Grégoire, J.-M. (2001). Detecting vegetation leaf water content using reflectance in the optical domain. *Remote Sensing of Environment, 77*(1), 22–33. https://doi.org/10.1016/S0034-4257(01)00191-2.

Cilia, C., Panigada, C., Rossini, M., Meroni, M., Busetto, L., Amaducci, S., et al. (2014). Nitrogen status assessment for variable rate fertilization in maize through hyperspectral imagery. *Remote Sensing, 6*(7), 6549.

Clark, R. N., & Roush, T. L. (1984). Reflectance spectroscopy: Quantitative analysis techniques for remote sensing applications. *Journal of Geophysical Research, 89*(B7), 6329–6340.

Danson, F. M., Steven, M. D., Malthus, T. J., & Clark, J. A. (1992). High-spectral resolution data for determining leaf water content. *International Journal of Remote Sensing, 13*(3), 461–470. https://doi.org/10.1080/01431169208904049.

Dawson, T. P., Curran, P. J., North, R. J., & Plummer, S. E. (1998). The propagation of foliar biochemical absorption features in forest canopy reflectance: A theoretical analysis. *Remote Sensing of Environment, 67,* 147–159.

Ding, C., Liu, X., Huang, F., Li, Y., & Zou, X. (2017). Onset of drying and dormancy in relation to water dynamics of semi-arid grasslands from MODIS NDWI. *Agricultural and Forest Meteorology, 234,* 22–30. https://doi.org/10.1016/j.agrformet.2016.12.006.

Feng, W., Qi, S., Heng, Y., Zhou, Y., Wu, Y., Liu, W., et al. (2017). Canopy vegetation indices from in situ hyperspectral data to assess plant water status of winter wheat under powdery mildew stress. *Frontiers in Plant Science*. https://doi.org/10.3389/fpls.2017.01219.

Gao, B. C. (1996). NDWI—A normalized difference water index for remote sensing of vegetation liquid water from space. *Remote Sensing of Environment, 58,* 257–266.

Hunt, E. R., Daughtry, C. S. T., Qu, J. J., Wang, L., & Hao, X. J. (2011) Comparison of hyperspectral retrievals with vegetation water indices for leaf and canopy water content. In *Remote sensing and modeling of ecosystems for sustainability VIII SPIE optical engineering + applications*, *San Diego, CA, 2011* (Vol. 8156, pp. 815606). SPIE

Hunt, E. R., & Rock, B. N. (1989). Detection of changes in leaf water content using near- and middle-infrared reflectances. *Remote Sensing of Environment, 30*(1), 43–54. https://doi.org/10.1016/0034-4257(89)90046-1.

Kim, D. M., Zhang, H., Zhou, H., Du, T., Wu, Q., Mockler, T. C., et al. (2015). Highly sensitive image-derived indices of water-stressed plants using hyperspectral imaging in SWIR and histogram analysis. *Scientific Reports, 5,* 15919. https://doi.org/10.1038/srep15919.

Kruse, F. A., Lefkoff, A. B., Boardman, J. B., Heidebrecht, K. B., Shapiro, A. T., Barloon, P. J., et al. (1993). The spectral image processing system (SIPS)—interactive visualization and analysis of imaging spectrometer data. *Remote Sensing of Environment, 44,* 145–163.

Liu, J., Miller, J. R., Pattey, E., Haboudane, D., Strachan, I. B., & Hinther, M. (2004) Monitoring crop biomass accumulation using multi-temporal hyperspectral remote sensing data. In *IGARSS 2004. 2004 IEEE international geoscience and remote sensing symposium*, *September 20–24, 2004* (Vol. 3, pp. 1637–1640 vol.1633). https://doi.org/10.1109/igarss.2004.1370643.

Mahlein, A. K., Steiner, U., Dehne, H. W., & Oerke, E. C. (2010). Spectral signatures of sugar beet leaves for the detection and differentiation of diseases. *Precision Agriculture*. https://doi.org/10.1007/s11119-010-9180-7.

Murphy, R. J. (2015). Evaluating simple proxy measures for estimating the depth of the ~ 1900 nm water absorption feature from hyperspectral data acquired under natural illumination. *Remote Sensing of Environment, 166,* 22–33.

Murphy, R. J., Tolhurst, T. J., Chapman, D. J., & Underwood, A. J. (2005). Remote-sensing of benthic chlorophyll: Should ground-truth data be expressed in units of area or mass? *Journal of Experimental Marine Biology and Ecology, 316,* 69–77.

Ollinger, S. V. (2011). Sources of variability in canopy reflectance and the convergent properties of plants. *New Phytologist, 189*(2), 375–394. https://doi.org/10.1111/j.1469-8137.2010.03536.x.

Pandey, P., Ge, Y., Stoerger, V., & Schnable, J. C. (2017). High throughput in vivo analysis of plant leaf chemical properties using hyperspectral imaging. *Frontiers in Plant Science*. https://doi.org/10.3389/fpls.2017.01348.

Penuelas, J., Filella, I., Biel, C., Serrano, L., & Save, R. (1993). The reflectance at the 950-970 nm region as an indicator of plant water status. *International Journal of Remote Sensing, 14*(10), 1887–1905.

Penuelas, J., Pinol, J., Ogaya, R., & Filella, I. (1997). Estimation of plant water concentration by the Reflectance Water Index WI (R900/R970). *International Journal of Remote Sensing, 18*(13), 2869–2875.

Rollin, E. M., & Milton, E. J. (1998). Processing of high spectral resolution reflectance data for the retrieval of canopy water content information. *Remote Sensing of Environment, 65,* 86–92.

Sankaran, S., Khot, L. R., Espinoza, C. Z., Jarolmasjed, S., Sathuvalli, V. R., Vandemark, G. J., et al. (2015). Low-altitude, high-resolution aerial imaging systems for row and field crop phenotyping: A review. *European Journal of Agronomy, 70,* 112–123. https://doi.org/10.1016/j.eja.2015.07.004.

Sankaran, S., Mishra, A., Ehsani, R., & Davis, C. (2010). A review of advanced techniques for detecting plant diseases. *Computers and Electronics in Agriculture, 72*(1), 1–13. https://doi.org/10.1016/j.compag.2010.02.007.

Serrano, L., Ustin, S., Roberts, D. A., Gamon, J. A., & Penuelas, J. (2000). Deriving water content of Chaparral vegetation from AVIRIS data. *Remote Sensing of Environment, 74,* 570–581.

Sims, D. A., & Gamon, J. A. (2003). Estimation of vegetation water content and photosynthetic tissue area from spectral reflectance: A comparison of indices based on liquid water and chlorophyll absorption features. *Remote Sensing of Environment, 84,* 526–537.

Steidle Neto, J. A., Lopes, D. D., & Borges Júnior, C. J. (2017). Assessment of photosynthetic pigment and water contents in intact sunflower plants from spectral indices. *Agriculture*. https://doi.org/10.3390/agriculture7020008.

Suárez, L., Zarco-Tejada, P. J., González-Dugo, V., Berni, J. A. J., Sagardoy, R., Morales, F., et al. (2010). Detecting water stress effects on fruit quality in orchards with time-series PRI airborne imagery. *Remote Sensing of Environment, 114*(2), 286–298. https://doi.org/10.1016/j.rse.2009.09.006.

Takala, T. L. H., & Mottus, M. (2016). Spatial variation of canopy PRI with shadow fraction caused by leaf-level irradiation conditions. *Remote Sensing of Environment, 182,* 99–112. https://doi.org/10.1016/j.rse.2016.04.028.

Tian, Q., Tong, Q., Pu, R., Guo, X., & Zhao, C. (2001). Spectroscopic determination of wheat water status using 1650-1850 nm spectral absorption features. *International Journal of Remote Sensing, 22*(12), 2329–2338. https://doi.org/10.1080/01431160118199.

Underwood, J., Wendel, A., Schofield, B., McMurray, L., & Kimber, R. (2017). Efficient in-field plant phenomics for row-crops with an autonomous ground vehicle. *Journal of Field Robotics, 34*(6), 1061–1083. https://doi.org/10.1002/rob.21728.

Vigneau, N., Ecarnot, M., Rabatel, G., & Roumet, P. (2011). Potential of field hyperspectral imaging as a non destructive method to assess leaf nitrogen content in Wheat. *Field Crops Research, 122*(1), 25–31. https://doi.org/10.1016/j.fcr.2011.02.003.

Wang, C., Nie, S., Xi, X., Luo, S., & Sun, X. (2017). Estimating the biomass of maize with hyperspectral and LiDAR data. *Remote Sensing, 9*(1), 11.

Wang, L. L., Hunt, E. R., Qu, J. J., Hao, X. J., & Daughtry, C. S. T. (2013). Remote sensing of fuel moisture content from ratios of narrow-band vegetation water and dry-matter indices. *Remote Sensing of Environment, 129,* 103–110. https://doi.org/10.1016/j.rse.2012.10.027.

Wang, X., Zhao, C., Guo, N., Li, Y., Jian, S., & Yu, K. (2015). Determining the canopy water stress for spring wheat using canopy hyperspectral reflectance data in loess plateau semiarid regions. *Spectroscopy Letters, 48*(7), 492–498. https://doi.org/10.1080/00387010.2014.909495.

Wendel, A., & Underwood, J. (2017). Illumination compensation in ground based hyperspectral imaging. *ISPRS Journal of Photogrammetry and Remote Sensing, 129,* 162–178.

Xiao, Y. F., Zhao, W. J., Zhou, D. M., & Gong, H. L. (2014). Sensitivity analysis of vegetation reflectance to biochemical and biophysical variables at leaf, canopy, and regional scales. *IEEE Transactions on Geoscience and Remote Sensing, 52*(7), 4014–4024. https://doi.org/10.1109/tgrs.2013.2278838.

Yang, C., & Everitt, J. H. (2012). Using spectral distance, spectral angle and plant abundance derived from hyperspectral imagery to characterize crop yield variation. *Precision Agriculture, 13*(1), 62–75. https://doi.org/10.1007/s11119-011-9248-z.

Yang, C., Everitt, J. H., Bradford, J. M., & Murden, D. (2004). Airborne hyperspectral imagery and yield monitor data for mapping cotton yield variability. *Precision Agriculture, 5*(5), 445–461. https://doi.org/10.1007/s11119-004-5319-8.

Yilmaz, M. T., Hunt, E. R., & Jackson, T. J. (2008). Remote sensing of vegetation water content from equivalent water thickness using satellite imagery. *Remote Sensing of Environment, 112,* 2514–2522.

Yu, K.-Q., Zhao, Y.-R., Li, X.-L., Shao, Y.-N., Liu, F., & He, Y. (2014). Hyperspectral imaging for mapping of total nitrogen spatial distribution in pepper plant. *PLoS ONE, 9*(12), e116205. https://doi.org/10.1371/journal.pone.0116205.

Zarco-Tejada, P. J., Berjón, A., López-Lozano, R., Miller, J. R., Martín, P., Cachorro, V., et al. (2005). Assessing vineyard condition with hyperspectral indices: Leaf and canopy reflectance simulation in a row-structured discontinuous canopy. *Remote Sensing of Environment, 99*(3), 271–287. https://doi.org/10.1016/j.rse.2005.09.002.

Zarco-Tejada, P. J., Catalina, A., González, M. R., & Martín, P. (2013a). Relationships between net photosynthesis and steady-state chlorophyll fluorescence retrieved from airborne hyperspectral imagery. *Remote Sensing of Environment, 136,* 247–258. https://doi.org/10.1016/j.rse.2013.05.011.

Zarco-Tejada, P. J., González-Dugo, V., & Berni, J. A. J. (2012). Fluorescence, temperature and narrow-band indices acquired from a UAV platform for water stress detection using a micro-hyperspectral imager and a thermal camera. *Remote Sensing of Environment, 117,* 322–337. https://doi.org/10.1016/j.rse.2011.10.007.

Zarco-Tejada, P. J., Guillén-Climent, M. L., Hernández-Clemente, R., Catalina, A., González, M. R., & Martín, P. (2013b). Estimating leaf carotenoid content in vineyards using high resolution hyperspectral imagery acquired from an unmanned aerial vehicle (UAV). *Agricultural and Forest Meteorology, 171–172,* 281–294. https://doi.org/10.1016/j.agrformet.2012.12.013.